

Eddy–Zonal Flow Feedback in the Southern Hemisphere

DAVID J. LORENZ AND DENNIS L. HARTMANN

Department of Atmospheric Sciences, University of Washington, Seattle, Washington

(Manuscript received 21 March 2000, in final form 22 May 2001)

ABSTRACT

The variability of the zonal-mean zonal wind in the Southern Hemisphere is studied using EOF analysis and momentum budget diagnostics of NCEP reanalysis data (1978–97). The leading EOF of the zonal-mean zonal wind is well separated from the remaining EOFs and represents the north–south movement of the midlatitude jet. Analysis of the momentum budget shows that a positive feedback between the zonal-mean wind anomalies and the eddy momentum fluxes accounts for the unusual persistence of EOF1 and plays an important role in the selection of the leading EOF of midlatitude variability. Further analysis also shows a propagating feedback, common to both EOF1 and EOF2, which is responsible for the poleward drift of wind anomalies with time. The observations support the following feedback mechanism. Anomalous baroclinic wave activity is generated at the latitude of anomalous temperature gradient that, by thermal wind, coincides with the latitude of the anomalous zonal jet. The net propagation of baroclinic wave activity away from the jet gives momentum fluxes into the jet. This positive feedback is partially offset by low-frequency, equivalent barotropic eddies that propagate into the jet and remove momentum from it. The bias toward equatorward wave propagation on a sphere contributes to the poleward drift of the wind anomalies.

1. Introduction

The variability of the zonal-mean state of the atmosphere has been a topic of research for a long time (Rossby 1939; Willett 1948; Namias 1950). Recently, as more reliable data became available, interest has shifted to the zonal-mean variability in the Southern Hemisphere (Trenberth 1979). Because of the greater symmetry of the Southern Hemisphere, the variations of the zonal-mean state represent a larger fraction of the total variability. The structure of the dominant mode of interannual variability of the zonal-mean wind is an equivalent barotropic dipole with maximum anomalies at 40° and 60°S (Kidson 1988; Karoly 1990; Nigam 1990; Hartmann and Lo 1998). These anomalies represent north–south fluctuations in the position of the zonal-mean midlatitude jet about its time mean position of 50°S. This mode of variability is very robust: the same pattern appears in daily, 10-day low-pass-filtered and monthly mean data, and in every season (Nigam 1990; Hartmann and Lo 1998). The timescales of the variations associated with this mode are quite long, with most of the variance at periods longer than 1 month (Hartmann and Lo 1998). The zonal index is a measure of the strength of this mode, and the two extreme states of the flow are called index states. The state with the

jet poleward of its mean position is called the high index state and vice versa.

The zonal index is essentially the same phenomenon that is measured by the leading mode of geopotential height on a constant pressure surface studied by Karoly (1990), Kidson and Sinclair (1995), and Sinclair et al. (1997). This “high-latitude mode” of the Southern Hemisphere is predominantly zonally symmetric and represents the fluctuation of mass between the polar regions and the midlatitudes, which must accompany the shift in midlatitude winds. Recently, Gong and Wang (1999) and Thompson and Wallace (2000) have noted the remarkable similarity between this Southern Hemisphere “annular mode” and the leading mode of sea level pressure in the Northern Hemisphere.

The zonal index is also found in many simple quasigeostrophic and primitive equation models with simple physics and no topography or seasonal cycle (Robinson 1991; James and James 1992; Yu and Hartmann 1993; Robinson 1994; Feldstein and Lee 1996; Lee and Feldstein 1996; Robinson 1996; Akahori and Yoden 1997). Realistic general circulation models with climatological forcing can simulate the observed structure and amplitude of both the northern and southern annular modes of variability (Limpasuvan and Hartmann 1999; Limpasuvan and Hartmann 2000). Because the external forcing for these models that produce an index cycle is independent of time, the variability found in these models is unforced variability associated with dynamic processes internal to the atmosphere. Recently there has

Corresponding author address: Mr. David J. Lorenz, Department of Atmospheric Sciences, Box 351640, University of Washington, Seattle, WA 98195.
E-mail: djlorenz@atmos.washington.edu

been some controversy regarding the mechanism responsible for this variability, in particular, the role of the eddies, or zonally asymmetric motions. It is well known that the eddies drive changes in the zonal-mean wind. The controversy is whether the changes in the zonal-mean flow have an important effect on the eddy momentum fluxes or, equivalently, whether there is an important zonal-mean wind–eddy feedback.

Various observational studies suggest that a zonal-mean wind–eddy feedback increases the persistence and low-frequency variance of the zonal index (Karoly 1990; Hartmann 1995; Kidson and Sinclair 1995; Hartmann and Lo 1998). Recently, Feldstein and Lee (1998) have questioned the importance of a positive feedback by the total eddy forcing in the variability of the atmospheric zonal index, although they did find evidence suggesting that the high-frequency eddies prolong the decay of zonal-mean wind anomalies. They also found, however, that the total effect of the eddies is significantly altered by the contributions from the low- and cross-frequency eddies, such that the eddies do not increase the persistence of the zonal index. Instead, Feldstein (1998) suggests that the eddy momentum fluxes cause a poleward propagation of the zonal-mean wind anomalies.

In the current study, we use momentum budget diagnostics to show that the total eddy momentum flux responds to the zonal wind anomalies. We also develop a method to quantify the effect of this response on the persistence and variance of the zonal wind anomalies. We then use this method to argue that the zonal wind–eddy feedback plays an important role in the selection of the leading mode of midlatitude variability. The paper begins with a brief discussion of the data and analysis (section 2), followed in section 3 by a short description of the annual mean zonal wind. In section 4 we discuss the leading EOF of the zonal-mean wind and diagnose its effect on the eddy momentum fluxes. In section 5 we describe a simple model of the zonal-mean wind–eddy feedback and use this model to estimate the effect of the feedback on the variability of the zonal wind. Section 6 describes the dynamics of the zonal wind–eddy feedback. In section 7, we apply the above analysis to the second EOF and discuss the role of the zonal wind–eddy feedback in the selection of the dominant mode of variability. The paper ends with the conclusion.

2. Data and analysis

For this study, we used Natural Centers for Environmental Prediction (NCEP) reanalysis daily wind and temperature data at constant pressure levels (Kalnay et al. 1996). We used data for the Southern Hemisphere from 1978 to 1997 on a 2.5×2.5 latitude–longitude grid and 12 vertical levels (1000, 925, 850, 700, 600, 500, 400, 300, 250, 200, 150, and 100 mb). For some parts of this study, we time filtered the daily data using a 10-day cutoff Lanczos filter with 41 weights (Ham-

ming 1989). We used the edges of the years 1977 and 1998 to properly filter the data for 1978–97.

To analyze the variability of the zonal-mean wind and the eddy fluxes, we found daily anomaly data by removing the mean seasonal cycle. The mean seasonal cycle is defined as the annual average and the first four Fourier harmonics of the 20-yr (1978–97) daily climatology. We then performed an EOF analysis for the zonal-mean zonal wind using the 20 years of daily anomaly data. For the EOF analysis, the data fields were properly weighted to account for the decrease of area toward the pole and the uneven spacing of pressure levels. The first and second EOFs are unique according to the North et al. (1982) test. We present the EOFs in meters per second and not in normalized form so that the magnitude of the structures can easily be seen. This is done by a regression of the anomaly data on the normalized principal component (PC) time series.

For the spectral analyses, we divided the input time series into 256 day sections overlapped by 128 days and windowed by a Hanning window. For a time series of length 7305 days this gave at least 57 degrees of freedom for the composite spectrum. We also used cross-spectrum analysis to find the phase relationship between two time series as a function of frequency. For this analysis, the coherence squared function is a measure of the consistency of the phase and amplitude relationship between the two time series over the sample.

For certain fields that vary in phase with the zonal index, we composited the fields for days when the zonal index exceeded 1.5 standard deviations from the mean, which yielded 411 days for the high index composite and 589 days for the low index composite.

3. Annual mean

Before looking at the variability of the zonal-mean zonal wind, it is helpful to look at the annual mean wind. Figure 1a shows a latitude–pressure plot of the annual average zonal-mean zonal wind. The wind is largest in the subtropical jet at 30°S and 200 mb. The midlatitude jet is at 50°S, where the strongest westerlies reach the surface. The distinction between these annual mean jets can be seen more clearly in constant pressure maps. At 200 mb (Fig. 1b), the subtropical jet stretching over Australia is about the same magnitude as the midlatitude jet over the southern Atlantic and Indian Oceans. Looking at monthly means (not shown), however, one sees that the subtropical jet is much stronger in July (maximum mean zonal wind is 55 m s^{-1}) and it almost disappears in January, whereas the midlatitude jet is nearly constant throughout the year (e.g., Hartmann and Lo 1998). At 500 mb (not shown), the subtropical jet weakens and the distinction between the jets becomes clearer, and at 850 mb (Fig. 1c) the subtropical jet is absent and the westerlies are confined to a relatively narrow band in the midlatitudes.

The differences in the low-level winds between the

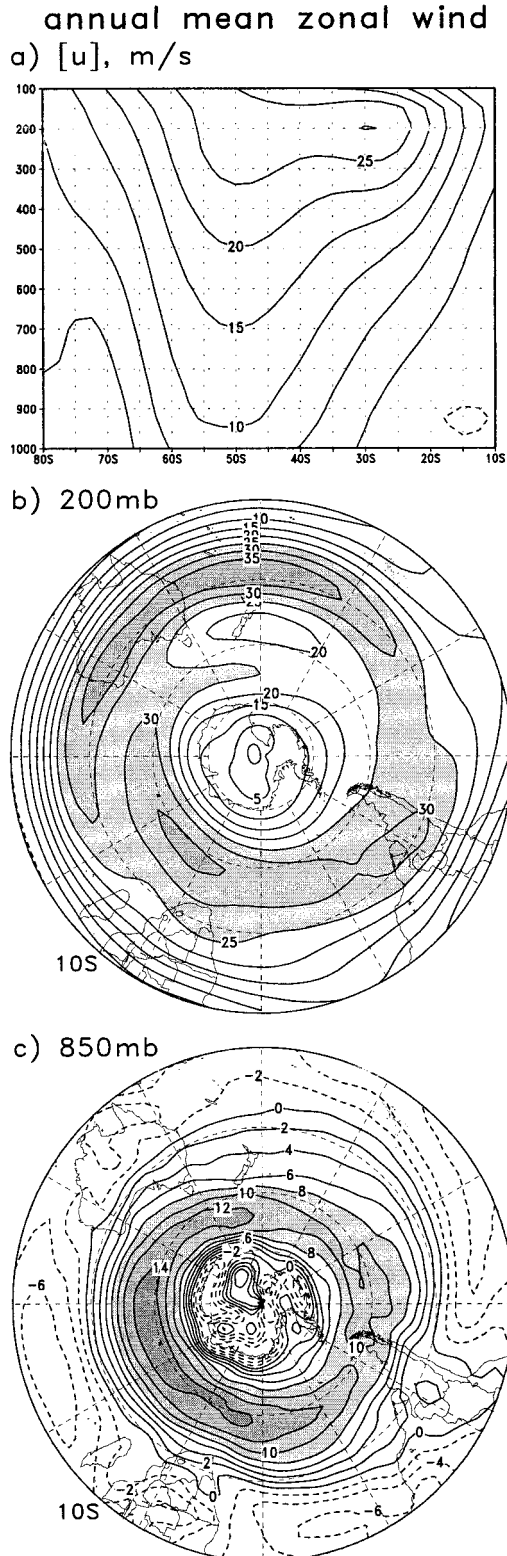


FIG. 1. Annual average westerly zonal wind (m s^{-1}). (a) Cross section of zonal-mean zonal wind; vertical axis is pressure (mb) and horizontal axis is latitude; (b) zonal wind at 200 mb; (c) zonal wind at 850 mb.

subtropics and the midlatitudes reflect the different dynamical processes that maintain the subtropical and midlatitude jet. The subtropical jet is driven by differential heating between the Tropics and subtropics, which creates a pressure gradient forcing air poleward at upper levels and equatorward at lower levels. The Coriolis force acting on the meridional wind gives westerlies at upper levels and easterlies at lower levels. Much of the variability of the subtropical jet is determined by the seasonal cycle of heating in the Tropics, giving a strong jet in winter and a weak jet in summer. In the midlatitudes, on the other hand, the eddies play an essential role by transporting westerly momentum from upper levels in the subtropics and midlatitudes to low levels in the midlatitudes. The source of the eddy activity is the instability associated with the temperature gradient in the lower troposphere of the midlatitudes. In the Southern Hemisphere, the relatively constant ocean temperatures play a major role in maintaining this gradient, and thus the seasonal cycle in the midlatitudes is small compared to the Northern Hemisphere. Therefore, a significant portion of the zonal-mean variability in the midlatitude Southern Hemisphere is associated with dynamical processes internal to the atmosphere and not with variability associated with the external seasonal cycle. It is this internal variability that is the focus of this paper.

4. Zonal wind–eddy feedback

The leading EOF of the daily zonal-mean zonal wind is an equivalent barotropic dipole with maximum anomalies at 40° and 60°S (Fig. 2a). The deep vertical structure of the wind anomalies suggest that this EOF is associated with the midlatitude jet and the eddies. Looking at the annual mean zonal wind (Fig. 1a), we see that the leading EOF represents north–south fluctuations in the position of the midlatitude jet about its time mean position of 50°S . This mode explains a significant amount of the total variance (36%). The PC time series associated with this leading EOF in the latitude–pressure plane is the same as the leading EOF of the vertically averaged zonal-mean zonal wind (Fig. 2; variance explained = 43%); the PC time series of the two modes are correlated at 0.998. Since the vertically averaged flow describes the variability, the direct effect of the eddies on the zonal-mean wind is the convergence of the vertically averaged eddy momentum flux (Hoskins 1983):

$$\frac{\partial \langle [u] \rangle}{\partial t} = -\frac{1}{\cos^2 \phi} \frac{\partial \langle [u'v'] \cos^2 \phi \rangle}{a \partial \phi} - F, \quad (1)$$

where $\langle u \rangle$ is the vertical average of u , $[u]$ is the zonal mean of u , u' is $u - [u]$, ϕ is the latitude, a is the radius of the earth, and F is the residual momentum forcing. The first term on the right will be called the eddy forcing. In the midlatitudes of the Southern Hemisphere, the residual momentum forcing F is dominated by boundary layer friction. To diagnose the effect of the eddies on

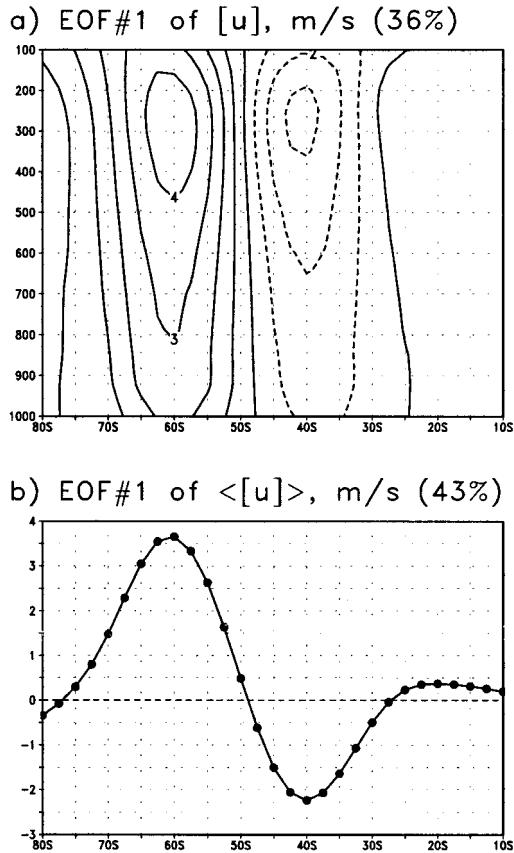


FIG. 2. (a) EOF1 of the zonal-mean zonal wind; (b) EOF1 of the vertical and zonal-mean zonal wind. The percent variance explained is given at top-right corner of plot.

the leading EOF of $\langle [u] \rangle$, we project the EOF pattern of $\langle [u] \rangle$ onto the vertically averaged eddy forcing anomalies. The resulting eddy forcing time series is called $m(t)$. For the remainder of this section, $z(t)$ is defined to be the zonal index (i.e., the leading PC of $\langle [u] \rangle$), $m(t)$ is the eddy forcing of the zonal index, capital letters denote the Fourier transform of the corresponding lower case variable, and A^* denotes the complex conjugate of A .

If z and m are linearly related, then relationship between z and m can be easily determined using cross-spectrum analysis. The ratio of the cross-spectrum ($=MZ^*$) to the z power spectrum ($=ZZ^*$) is plotted in Fig. 3a. The imaginary part is quite close to the angular frequency ω , and the real part is nearly constant at low frequencies. This implies that $M = (\tau^{-1} + i\omega)Z$ or, equivalently,

$$\frac{dz}{dt} = m - \frac{z}{\tau}, \quad (2)$$

where τ is a constant. This is the equation that would be obtained if F in (1) was parameterized by Rayleigh damping with a decay timescale of τ . The large coherence squared (Fig. 3b) demonstrates that (2) is a good approximation. The phase difference between z and m

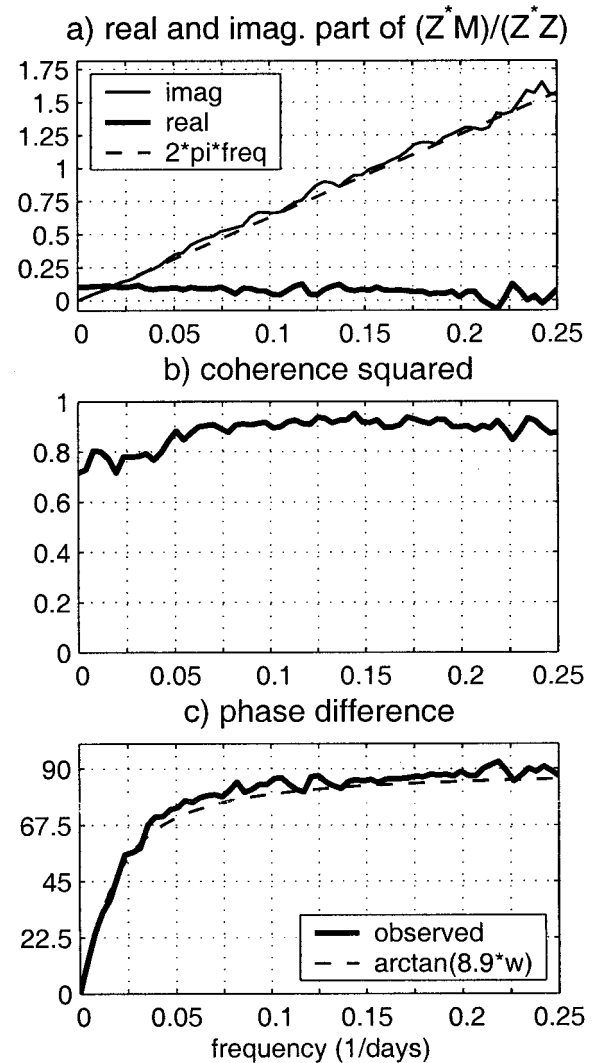


FIG. 3. Cross-spectrum analysis between z and m : (a) real and imaginary part of the cross-spectrum divided by the z power spectrum, and the expected imaginary part; (b) coherence squared; (c) phase difference between m and z . Positive phase difference means m leads z . Horizontal axis is frequency for all plots.

(Fig. 3c) is about 90° for most frequencies but approaches zero at low frequencies. The expected phase difference between z and m implied by (2), $\arctan(\omega\tau)$, matches the observed phase difference when the Rayleigh damping timescale τ is 8.9 days (see appendix A). Equation (2) implies that the phase relationship between the eddy forcing and the zonal wind is constrained by momentum conservation. Thus, in the presence of dissipation, the eddy forcing always becomes more in phase with the zonal-mean wind at low frequencies. Therefore, composites of zonal-mean momentum fluxes in a high or low index state will always show reinforcing momentum fluxes regardless of whether there is a feedback. Also, because the eddies drive changes in the zonal-mean wind, the eddy forcing always leads the

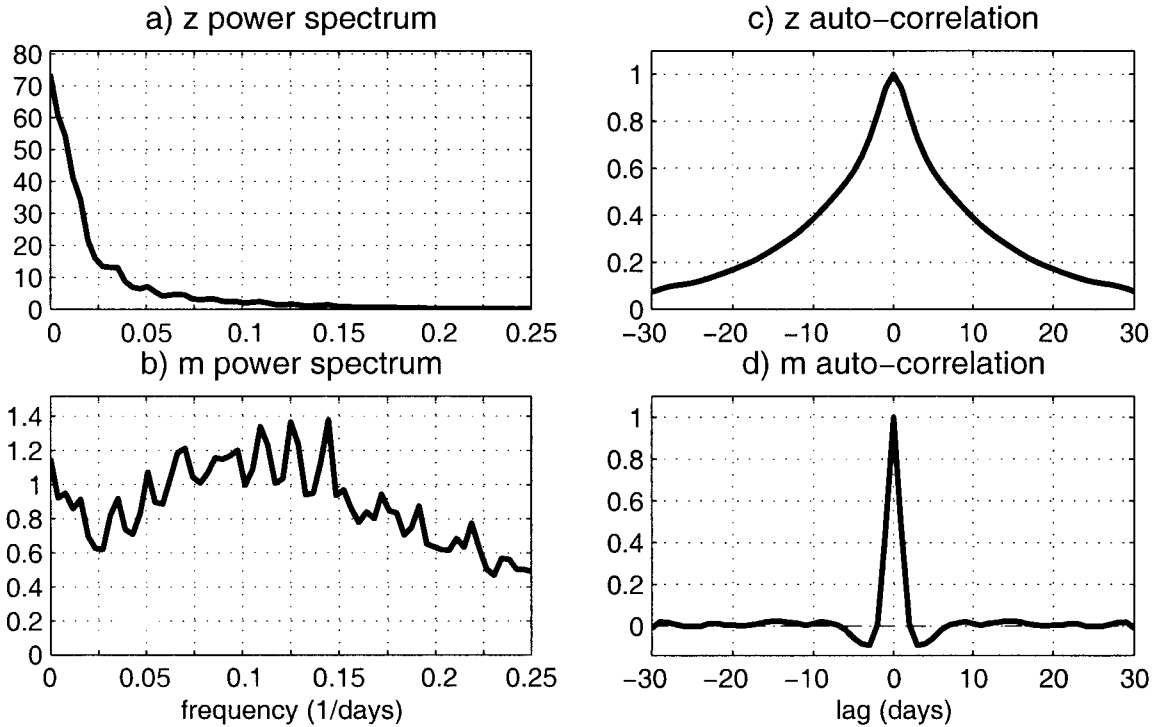


FIG. 4. Summary statistics for z and m . Power spectrum of (a) z and (b) m . Vertical axis is power spectral density in (a) $\text{m}^2 \text{s}^{-2}$ (b) and $\text{m}^2 \text{s}^{-2} \text{day}^{-2}$; Autocorrelation of (c) z and (d) m .

zonal-mean wind by 0° to 90° . Therefore, composites of zonal index “events” will always show the largest eddy momentum fluxes prior to the largest zonal-mean wind anomalies (Robinson 1994, 1996; Feldstein and Lee 1996, 1998).

A summary of the basic characteristics of the time series z and m is given in Fig. 4. The most obvious difference between z and m is the characteristic timescale: z is much lower frequency than m (Figs. 4a,b). This is the expected relationship between a quantity, z ,

and its forcing, m . Looking at Fig. 4d we see that the eddy forcing autocorrelation is not a simple impulse; instead it has negative values at low lags. This feature is represented in the power spectrum (Fig. 4b) by the broad maximum centered at a frequency of 0.1 day^{-1} . Since z varies at such long timescales and, moreover, since there is no similar maximum in z (Fig. 4a), this feature is most likely an intrinsic characteristic of the eddy momentum forcing independent of the zonal-mean wind variability. To diagnose the effect of z on m , we look at the cross correlation between z and m (Fig. 5). First note that although the cross-spectrum analysis indicated that the two time series are very coherent, the correlations in Fig. 5 are small—the highest correlation is 0.5—because of the large differences in the timescale between z and m (Figs. 4a,b). As expected from (2), the strongest correlations are at short negative lags where the eddy forcing leads the zonal wind anomalies. The negative correlations at positive lags do not represent a negative feedback but are an artifact related to the eddy forcing only: the eddy forcing anomalies are negatively autocorrelated at small lags (Fig. 4d). To find evidence for a feedback, one must look for nonzero correlations at large positive lags. In this case, the correlations are small but consistently positive at large lags. These correlations implying a positive feedback are significant at the 95% level for lags of 6–13 days (see appendix B) and, moreover, are reproducible in subsamples of the 7305-day time series (not shown). We will show in the

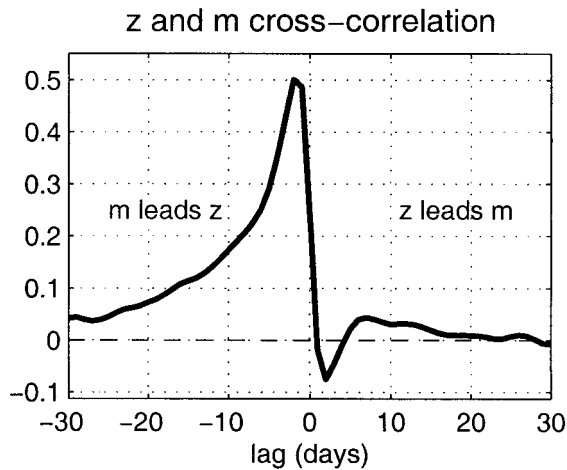


FIG. 5. Cross correlation between z and m .

next section that this positive feedback has a significant effect on z .

Before moving on to the next section, we address the subtlety of diagnosing a feedback from observations. Specifically we address the following question: do the correlations at large positive lags in Fig. 5 result from intrinsic eddy variability or do they result from a positive zonal wind–eddy feedback? First, the correlations at large positive lags are equivalent to the “redness” in the eddy forcing spectrum at periods longer than 40 days (Fig. 4b). One could argue that this redness is an intrinsic characteristic of the eddy variability independent of the zonal-mean wind, so that the positive correlations in Fig. 5 do not imply a positive feedback. Using time filtering, however, we can demonstrate that this redness does in fact result from a positive feedback. First, we use a 10-day cutoff Lanczos filter to divide both the eddy component of zonal wind, u' , and the eddy component of meridional wind, v' , into high- and low-frequency parts: u'_h , u'_l , v'_h and v'_l . The momentum flux by the eddies will then be divided into two parts: the flux by the high-frequency eddies [$u'_h v'_h$] and the flux by the low- and cross-frequency eddies [$u'_h v'_l + u'_l v'_h + u'_l v'_l$]. To avoid confusion later on, we will call the forcing by the high-frequency eddies the synoptic-eddy forcing and the forcing by the low- and cross-frequency eddies the residual-eddy forcing. The power spectra of the synoptic- and residual-eddy contribution to m (Fig. 6) show somewhat surprising features: the synoptic-eddy forcing clearly dominates over the residual-eddy forcing at low frequencies. Moreover, the redness in the synoptic-eddy forcing is much like the redness in the zonal-mean wind (Fig. 4a). Since the synoptic eddies consist of fluctuations in u' and v' of periods less than 10 days, yet their zonal-mean momentum forcing varies at the longest timescales, the synoptic-eddy forcing must be organized by the changes in the zonal-mean wind and, consequently, the redness in the total eddy forcing is due to a positive feedback with the zonal-mean wind.

5. Simple model of feedback

In this section, we describe a simple linear model of the zonal wind–eddy feedback that allows us to make a quantitative estimate of the strength of the feedback and its effect on the zonal-mean wind variance. The model also demonstrates the value of time-lagged regressions (or composites) rather than simultaneous regressions (or composites) for diagnosing the effect of the changes in the zonal-mean wind on the eddies.

Using cross-spectrum analysis, we empirically found that the zonal index (z) and the eddy momentum forcing (m) are approximately related by (2), which implies that F in (1) can be parameterized by Rayleigh damping. The empirical value for τ is 8.9 days (see appendix A).

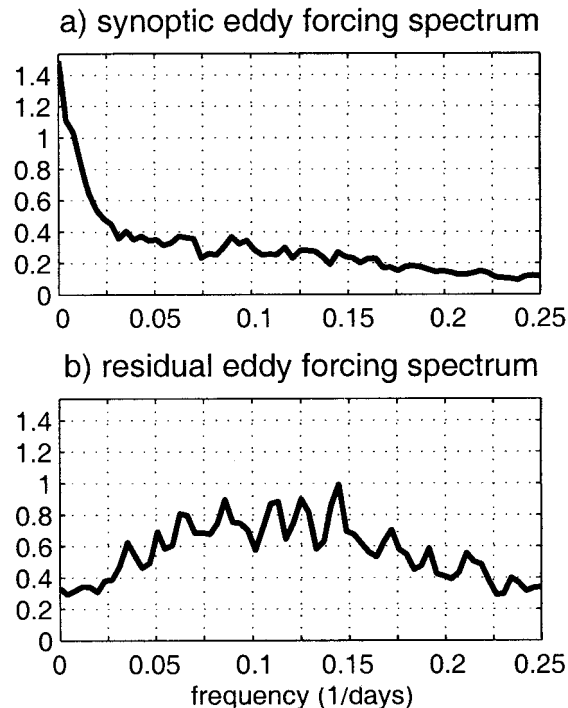


FIG. 6. Power spectra of the zonal index forcing by the time-filtered eddies: (a) synoptic-eddy forcing and (b) residual-eddy forcing. Vertical axis is power spectral density in $\text{m}^2 \text{s}^{-2} \text{day}^{-2}$.

To model the eddy feedback, assume that the changes in zonal wind cause an eddy forcing anomaly proportional to the wind anomalies; that is, assume that

$$m = \tilde{m} + bz, \quad (3)$$

where \tilde{m} is “random” eddy forcing independent of the zonal wind anomalies and b is a constant that measures the strength of the feedback. Let \tilde{z} be the zonal index in the absence of the feedback. Thus, if we assume that τ does not depend on the feedback, then \tilde{z} must be defined by

$$\frac{d\tilde{z}}{dt} = \tilde{m} - \frac{\tilde{z}}{\tau}. \quad (4)$$

In appendix C, we derive the cross-covariance between \tilde{z} and \tilde{m} from the observed cross-covariance (i.e., between z and m) using (2), (3), and (4). The constant b is determined such that the cross-covariance “without the feedback” is zero when \tilde{z} leads \tilde{m} by over a week. With a value for b , we can then find the power spectra and variance of z and m without the feedback (i.e., with $b = 0$).

The basic assumption of this feedback model is that the eddy forcing anomalies do not have long-term memory independent of the variability in the zonal wind (by (2), memory in the eddy forcing is equivalent to positive correlations at large lags in Fig. 5). The basis for this assumption appears at the end of section 4, where we argue that most of the variability in synoptic-eddy forc-

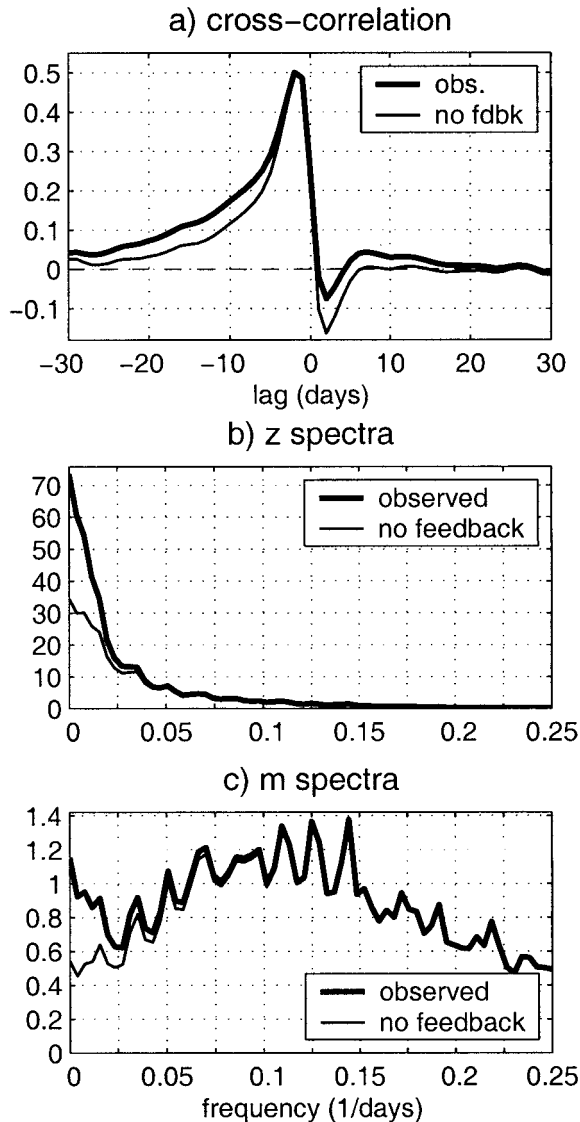


FIG. 7. Observed statistics (thick line) and calculated statistics for no feedback (thin line): (a) cross correlation between z and m and between \tilde{z} and \tilde{m} ; positive lag means z leads m ; (b) power spectra of z and \tilde{z} ; (c) power spectra of m and \tilde{m} .

ing at long timescales must be organized by variability in the zonal-mean wind. The free parameter b eliminates memory from the observed eddy forcing time series, m .

Figure 7a shows the observed cross correlation between the zonal index and the eddy forcing and the cross correlation with the feedback removed. The value of b is 0.0354 day^{-1} . Figures 7b and 7c show the calculated effect of the feedback on the zonal-mean wind and eddy forcing variability, respectively. At the lowest frequencies the feedback increases the variance of z by a factor of 2.1.¹ The total variance of z increases by 40%. The

¹ The factor 2.1 comes from the limit $\omega \rightarrow 0$ of C14, which is $[1 - \tau b]^{-2}$.

total variance of m only increases by 5% because m is dominated by high frequencies. Thus, the feedback has a relatively small effect on the eddy forcing variability: the m autocorrelation still appears to be local in time, like an impulse (Fig. 4d). The small positive bias at large lags in the m autocorrelation, however, has a pronounced effect on the variability of the zonal-mean wind.

The strength of the feedback, b ($=0.0354 \text{ day}^{-1}$), seems reproducible in subsamples of the total data record. For example, the estimated b for the first and second half of the dataset is 0.0354 and 0.0372 day^{-1} , respectively. It is also interesting to look at the seasonality of the feedback for EOF1. First, since the leading EOF of the zonal-mean wind is independent of season (e.g., Hartmann and Lo 1998), we can simply divide the z and m indices into summer (Nov–Apr) and winter (May–Oct) seasons. The calculated b using the cross-correlation function is larger for winter ($=0.0399 \text{ day}^{-1}$) than for summer ($=0.0336 \text{ day}^{-1}$). However, while the difference between winter and summer ($\sim 17\%$) is larger than the difference between the first and second half of the record ($\sim 5\%$), it is not clear if this difference is significant.

The simple linear model described in this section also has important implications for the interpretation of simultaneous regressions of eddy statistics on the zonal index (or, similarly, for composites of eddy statistics during “high” and “low” index states of the zonal index). Simultaneous regressions are not a good way to diagnose the effect of the zonal-mean wind anomalies on the eddies because only a small fraction of the eddy momentum flux anomalies at zero time lag are attributable to the zonal wind anomalies. As demonstrated in appendix D, only 31% ($=\tau b$) of the simultaneous eddy momentum forcing anomalies are caused by changes in the zonal-mean flow (i.e., most of the eddy forcing is associated with the \tilde{m} part of m). In order to assess the effect of the zonal wind anomalies on the eddies, one must therefore look at positive lags greater than a week, where all of the eddy momentum flux anomalies are caused by the changes in the zonal-mean wind. These ideas on the interpretation of simultaneous composites and regressions are also stated in Feldstein and Lee (1996, 1998), Lee and Feldstein (1996), and Robinson (1996).

6. Dynamics of the feedback

The results from the previous section imply that in order to diagnose the effect of the zonal-mean wind anomalies on the eddies we must look at longer timescales. We need to isolate that part of the eddy forcing that persists for more than an eddy lifetime after a zonal flow anomaly has peaked. To this end we do time-lagged regressions of anomalous eddy fluxes on the zonal index (i.e., PC1 of the zonal-mean zonal wind). The point of the time lag is to isolate the part of the eddy forcing

that is responding to the zonal wind anomalies from the burst of eddy forcing that initially created the zonal wind anomalies. The results are well characterized by the regression of the eddy fluxes with wind anomalies that occurred 12 days earlier.

First, we divide the eddy fields using time filtering as in the end of section 3. The “synoptic” eddy forcing anomalies (Fig. 8a) generally reinforce the wind anomalies at 60° and 40°S. The synoptic-eddy forcing anomaly pattern, however, does not perfectly match the zonal wind anomaly pattern (Fig. 2b): the eddy forcing minimum is slightly poleward of 40°S and an additional eddy forcing maximum is evident in the subtropics. The anomalous synoptic-eddy momentum fluxes and Eliassen–Palm (EP) flux vectors (Edmon et al. 1980) that yield the above forcing are shown in Fig. 8b. The EP flux vectors show enhanced wave activity generation at low levels in the region of positive wind anomalies and inhibited wave generation at low levels in the region of negative wind anomalies. This pattern suggests that baroclinic wave generation, or, equivalently, low-level eddy temperature flux, follows the north–south movement of the upper-level jet, which, by thermal wind, implies that the wave generation follows the maximum temperature gradient. To diagnose this movement of “baroclinicity” we composite the meridional temperature gradient divided by the buoyancy frequency $[(g\theta_y)/(\theta_0 N)]$; this is proportional to the Eady (1949) wave growth rate] at 850 mb during the high and low index (Fig. 8c). During the high (low) index, the maximum midlatitude baroclinicity, which is basically determined by the temperature gradient, is poleward (equatorward) of its time mean position. Once waves are generated in the region of positive wind anomalies (i.e., above normal baroclinicity), they tend to propagate upward and then equatorward from the wave source (Fig. 8b). Thus the momentum flux anomalies are not symmetric about the latitude of the maximum wind anomalies but are strongest equatorward of the wind anomalies. This bias toward equatorward wave propagation or, equivalently, poleward momentum fluxes, results from spherical geometry (Balasubramanian and Garner 1997; Whitaker and Snyder 1993).

The above EP flux anomalies suggest a mechanism for the zonal wind–eddy feedback: the source of baroclinic wave activity follows the north–south movement of baroclinicity that, by thermal wind, generally corresponds to the latitude of strongest upper-level jet. The propagation of wave activity away from the jet gives momentum fluxes into the jet. Also, the prevalence of equatorward wave propagation yields a maximum eddy forcing anomaly slightly poleward of the wind anomaly at 40°S.

The above scenario only applies to that portion of the eddy fluxes that interact with the zonal wind anomalies. Clearly much of the variability in eddy activity is independent of the changes in the zonal-mean flow and

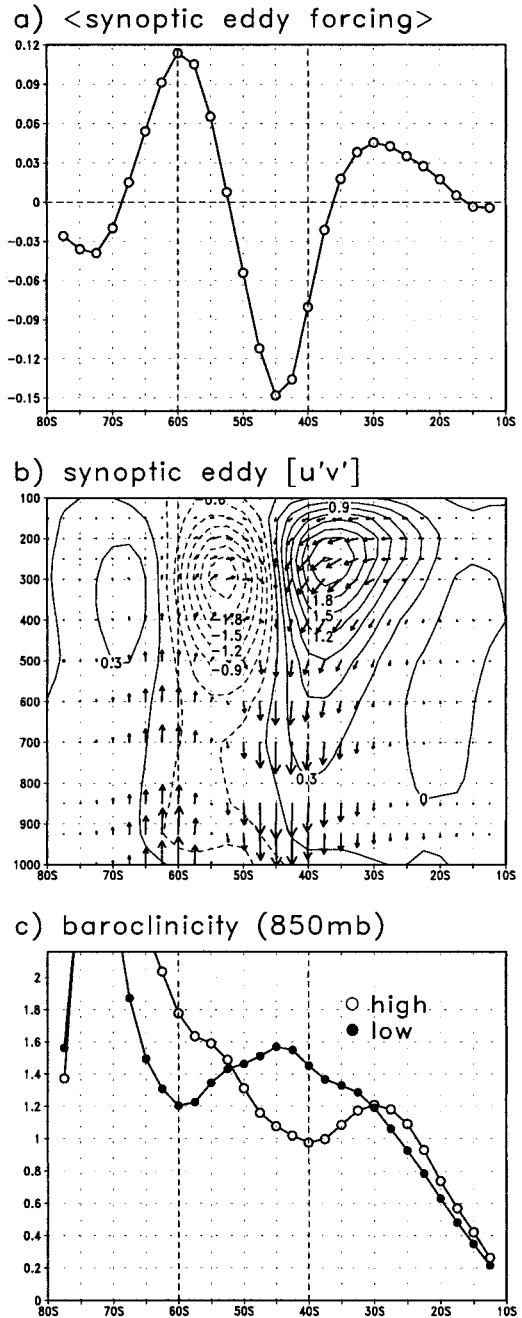


FIG. 8. (a) Anomalous vertical and zonal average synoptic-eddy momentum flux convergence regressed on PC1 of $\langle [u] \rangle$; PC1 leads by 12 days; vertical axis is $\text{m s}^{-1} \text{ day}^{-1}$. (b) Anomalous zonal-mean synoptic-eddy momentum flux and EP flux vectors regressed on PC1; PC1 leads by 12 days. (c) Composite baroclinicity $[(g\theta_y)/(\theta_0 N)]$ at 850 mb during high and low index; vertical axis is day^{-1} ; latitudes of the EOF1 wind anomalies are marked by vertical dashed lines.

drives the anomalous zonal wind and baroclinicity in the first place.

The calculations of Robinson (2000) provide more insight into the above feedback mechanism by including both the direct effect of the anomalous eddy fluxes as

well as the indirect effect of the eddies on the meridional circulation via anomalous friction and diabatic heating. His results show that forcing anomalies imply a meridional circulation that reinforces the low-level baroclinicity of the jet. This creation of low-level baroclinicity by the meridional circulation is crucial for the positive feedback because the direct effect of the eddies is to make the flow more barotropic. He also argues that the bias toward equatorward wave propagation tends to cause a poleward drift of the region of strongest baroclinicity.

Previous studies (Robinson 1991; Feldstein and Lee 1998) have noted that the “residual” eddy momentum fluxes are not simply random forcing of the zonal index but that a portion of the residual-eddy fluxes systematically acts to decay the zonal wind anomalies. One can infer that such a relationship exists by noting that the low-frequency variance of the synoptic-eddy forcing (Fig. 6a) is greater than the total eddy forcing (Fig. 4b). Thus, the residual-eddy forcing must be coherently out of phase with the synoptic-eddy forcing. The magnitude of the residual-eddy forcing anomalies (at a time lag of 12 days) is shown in Fig. 9a. The response of the residual eddies to the zonal-mean flow is dominated by the low-frequency eddies.² The anomalous residual-eddy momentum fluxes and EP flux vectors are shown in Fig. 9b. In contrast to the synoptic eddies, the residual-eddy momentum fluxes extend through the depth of the troposphere with relatively little change of amplitude and, moreover, the residual-eddy temperature fluxes are relatively small. This suggests that the residual eddies are predominantly external Rossby waves. Figure 9c shows the meridional profile of the external Rossby wave index of refraction $[(\beta - [u]_{yy})/([u] - c)]$ at the equivalent barotropic level during the high and low index.³ The index of refraction is largest at the latitude of the jet, implying a net propagation of Rossby waves into the jet accompanied by momentum fluxes out of the jet. The low-frequency, barotropic eddies thus consistently act to damp the jets created by the baroclinic eddies.

The total eddy momentum forcing (Fig. 10a), like the synoptic-eddy forcing, reinforces the zonal wind anomalies but is weaker and more confined to the upper troposphere (Fig. 10b) because of the canceling effect of the residual-eddy forcing. The relation between the total eddy forcing and the anomalous zonal flow also implies a poleward propagation of the zonal wind anomalies.

² The cross-frequency eddy forcing is essentially random forcing independent of the zonal index; the negative cross correlation (not shown) at small time lags after the maximum wind anomalies simply results from the quasi-periodic nature of the cross-frequency eddy forcing.

³ The equivalent barotropic level is taken to be 300 mb. The phase speed of the waves, c , is taken to be 2 m s^{-1} and is calculated from one point lag correlation plots of low-frequency meridional wind. The results do not depend strongly on these parameters. Also, spherical effects on index of refraction are considered for Fig. 9c.

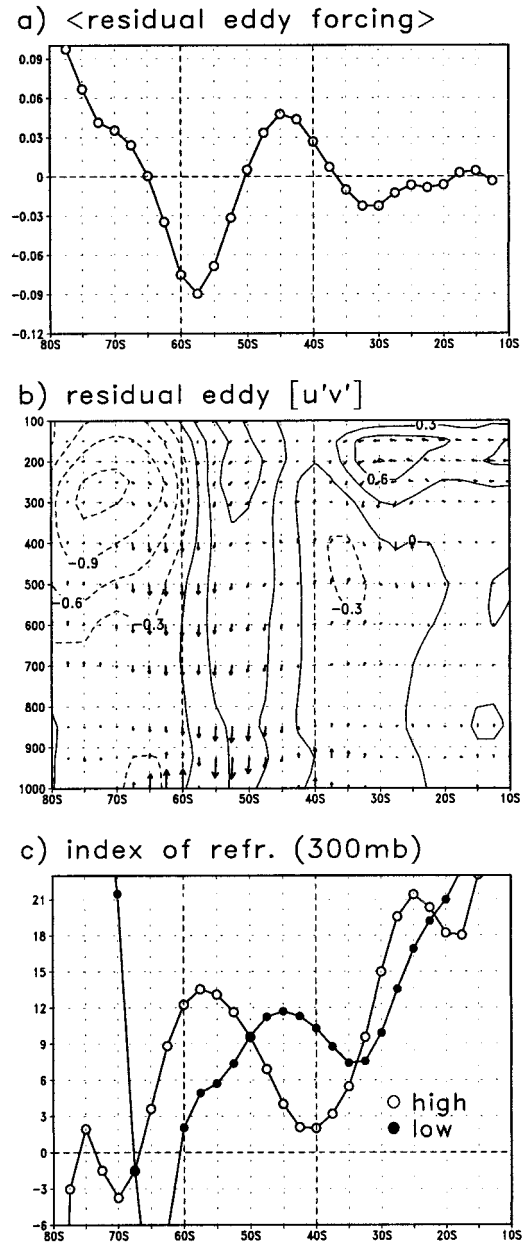


FIG. 9. (a) Anomalous vertical and zonal average residual-eddy momentum flux convergence regressed on PC1 of $\langle [u] \rangle$; PC1 leads by 12 days; vertical axis is in $\text{m s}^{-1} \text{ day}^{-1}$. (b) Anomalous zonal-mean residual-eddy momentum flux and EP flux vectors regressed on PC1; PC1 leads by 12 days. (c) Composite external Rossby wave index of refraction $[(\beta - [u]_{yy})/([u] - c)]$ at 300 mb during high and low index; vertical axis is in 10^{-13} m^{-2} ; latitudes of the EOF1 wind anomalies are marked by vertical dashed lines.

The poleward propagation at 40°S is present in the synoptic-eddy forcing (Fig. 8a), whereas the poleward propagation at 60°S results from a combination of effects: the synoptic-eddy forcing is largest at 60°S (Fig. 8a) but the residual-eddy forcing is largest (i.e., most negative) equatorward of 60°S (Fig. 9a). The total eddy momentum flux (Fig. 10b) also implies a significant

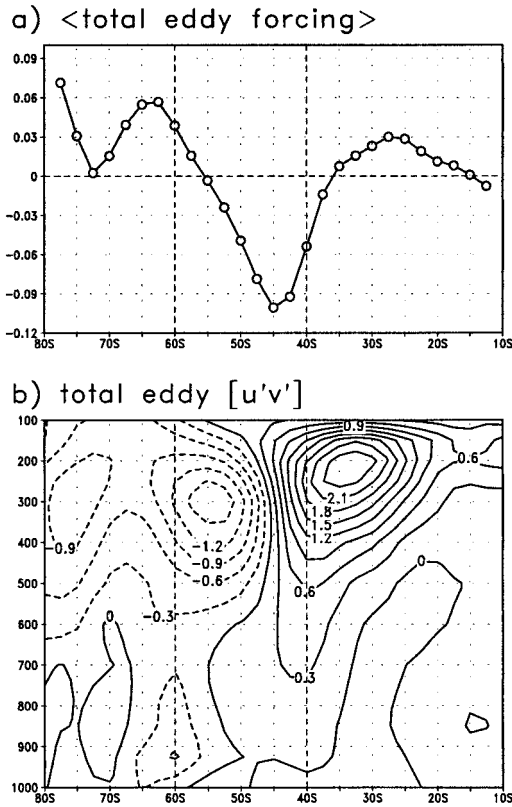


FIG. 10. (a) Anomalous vertical and zonal average total eddy momentum flux convergence regressed on PC1 of $\langle [u] \rangle$; PC1 leads by 12 days; vertical axis is in $\text{m s}^{-1} \text{ day}^{-1}$. (b) Anomalous zonal-mean total eddy momentum flux regressed on PC1; PC1 leads by 12 days; latitudes of the EOF1 wind anomalies are marked by vertical dashed lines.

remote response in the subtropics. In the high index, the eddies transport less momentum out of the subtropics, implying a weaker meridional circulation, less subsidence in the subtropics, and cooler midtropospheric temperatures in the subtropics. The effect of the eddy feedback on the zonal-mean circulation can be seen by regressing the zonal-mean wind anomalies on the zonal index at 0- and 20-day time lag (Fig. 11). Twenty days after the maximum wind anomalies at 40° and 60°S, the anomalies have drifted poleward by 2.5° and the subtropical anomaly is much more important relative to the midlatitude anomalies than at lag 0. The asymmetry in time of the development of the subtropical wind anomaly is even more clear if one uses the annular mode index (Thompson and Wallace 2000) instead of PC1 of the zonal-mean wind. In summary, the zonal wind anomalies associated with EOF1 have an important effect on the eddy momentum forcing. Part of the eddy forcing projects onto EOF1 increasing the persistence of the wind anomalies, and part of the eddy forcing is in quadrature with EOF1 causing poleward propagation of the wind anomalies.

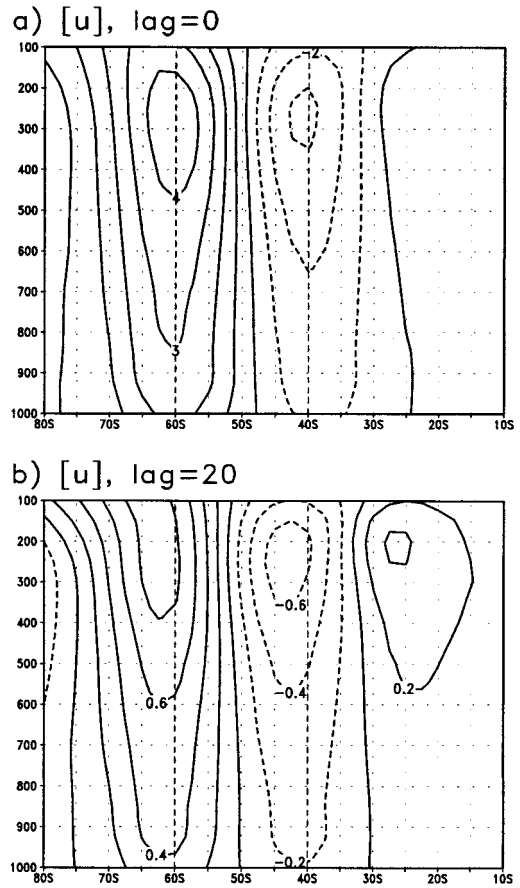


FIG. 11. Anomalous zonal-mean zonal wind regressed on PC1 of $\langle [u] \rangle$: (a) simultaneous and (b) PC1 leads by 20 days. Latitudes of the EOF1 wind anomalies are marked by vertical dashed lines.

7. EOF2

The above analysis was also performed on EOF2 of the zonal-mean zonal wind (Fig. 12a). The positive phase of this EOF corresponds to the strengthening and sharpening of the midlatitude jet. Like the first EOF, the second EOF of the vertical and zonal average zonal wind captures the variability of the second EOF in the latitude–pressure plane (correlation coefficient between the PCs = 0.995). The cross correlation between PC2 of the zonal wind and its eddy forcing is very similar to the cross correlation between PC1 (i.e., the zonal index) and the eddy forcing with the feedback removed (Fig. 13a). The cross correlation for EOF2, unlike EOF1, is not consistently positive for large positive lags (the positive correlations around lag 10 are not consistent across the time period and are most likely statistical noise). This cross correlation suggests that a positive zonal wind–eddy feedback does not exist for EOF2. Moreover, the autocorrelation (Fig. 13b) of PC2 is very similar to PC1 with the feedback removed, implying that the positive feedback accounts for the greater persistence of PC1 compared to PC2. The large persistence associated

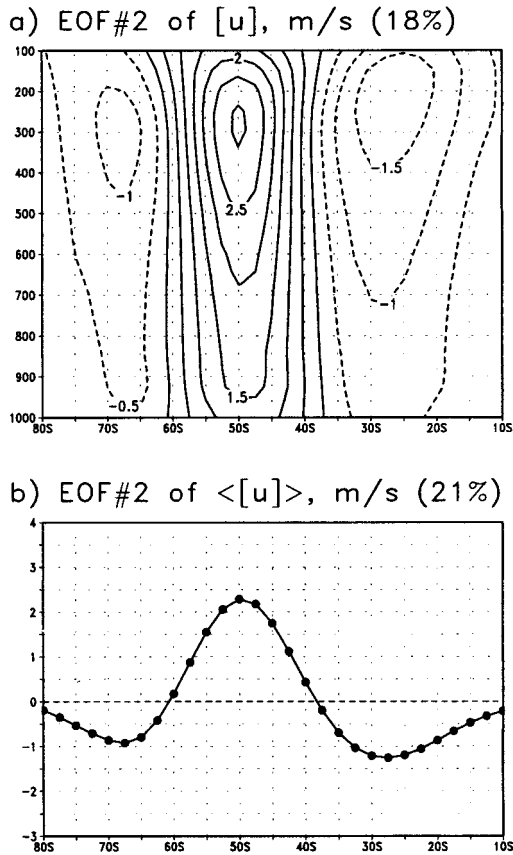


FIG. 12. (a) EOF2 of the zonal-mean zonal wind; (b) EOF2 of the vertical and zonal-mean zonal wind. The percent variance explained is given at top right corner of plot.

with north-south shifts of the midlatitude jet versus other modes of midlatitude variability is even more evident in simple general circulation models (e.g., James and James 1992). Moreover, the power spectra in their paper (their Fig. 6) suggest that this persistence accounts for the greater variance of EOF1 than EOF2 and thus the selection of the dominant mode. Looking at the power spectra in the atmosphere (Fig. 13c), we see that the feedback accounts for the majority of the excess variance of PC1 compared to PC2 at low frequencies. The positive feedback does not account for all the differences in variance (Fig. 13c), but since the feedback accounts for the persistence (Fig. 13b) the remaining variance must be explained by eddy forcing with no temporal autocorrelation (i.e., white noise). Thus the difference in variance between PC1 and PC2 results from 1) a positive zonal wind-eddy feedback on PC1, which is most important at low frequencies; and 2) the differing strengths of the random eddy forcing impulses driving EOF1 and EOF2, which effect all frequencies equally. The feedback increases the total variance of PC1 over that of PC2 by a factor of 1.4 (see section 5) and the impulsive eddy forcing increases the total var-

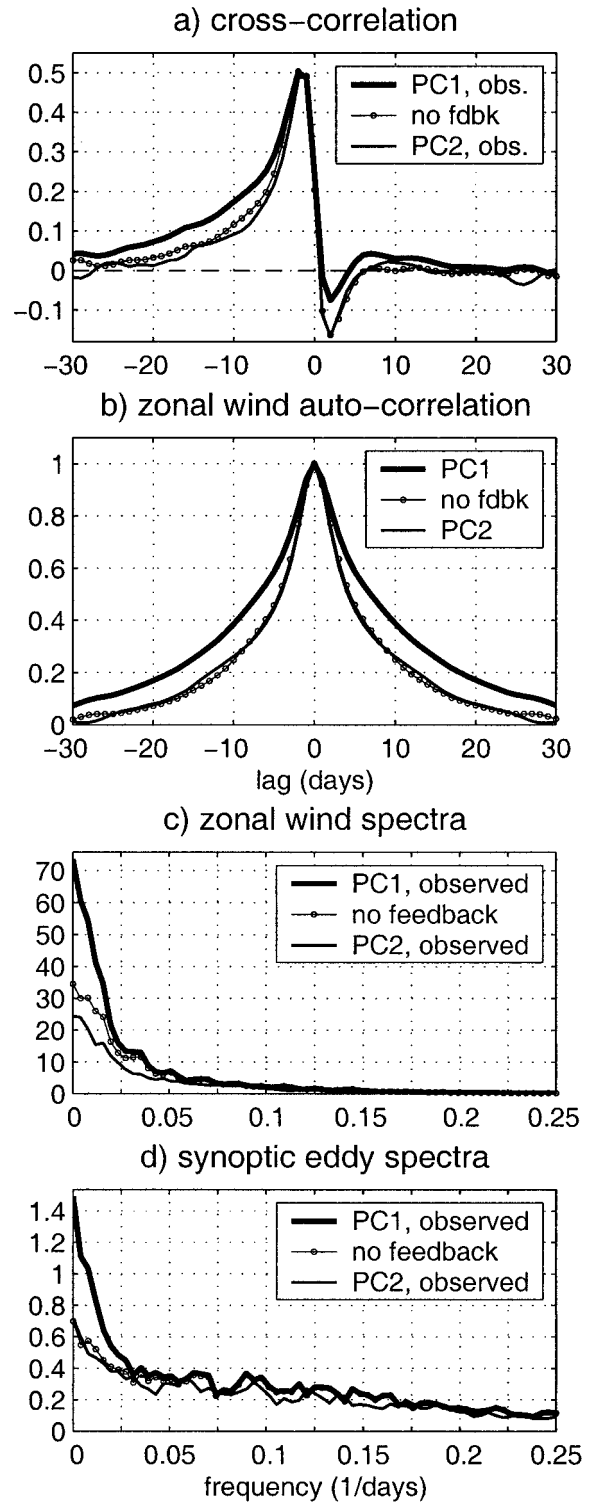


FIG. 13. Comparisons for EOF1, EOF1 without the feedback, and EOF2: (a) cross correlation between zonal-mean wind and eddy forcing; (b) autocorrelation for zonal-mean wind; (c) power spectra for zonal-mean wind; (d) power spectra for synoptic-eddy forcing of zonal-mean wind.

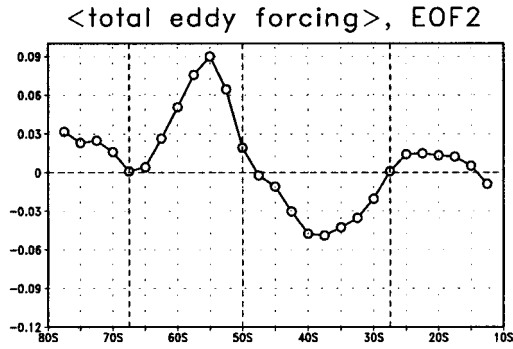


FIG. 14. Anomalous vertical and zonal average total eddy momentum flux convergence regressed on PC2 of $\langle [u] \rangle$; PC2 leads by 12 days; vertical axis is in $\text{m s}^{-1} \text{ day}^{-1}$; latitudes of the EOF2 wind anomalies are marked by vertical dashed lines.

iance by a factor of 1.5, so that the total variance of PC1 is greater by a factor of 2.1 ($=1.4 \times 1.5$).⁴

The difference in the positive eddy feedback between EOF1 and EOF2 can be easily be seen in the synoptic-eddy power spectrum (Fig. 13d). Thus, the synoptic eddies and not the residual eddies account for the differences in the total eddy positive feedback. Although the above results do not suggest a positive EOF2–eddy feedback, there does seem to be a propagating EOF2–eddy feedback (Fig. 14; cf. Fig. 12b; see also Feldstein 1998). Note that the time-lagged eddy forcing anomalies associated with EOF2 are in quadrature with the initial wind anomalies in the sense to cause a poleward propagation of the wind anomalies. The effect of this propagating feedback on EOF2 can be seen by regressing the zonal-mean wind anomalies on PC2 at 0- and 20-day time lag (Fig. 15). The effect of the feedback is quite pronounced: 20 days after the maximum wind anomalies at 50° and 27.5°S, the anomalies have drifted poleward by 10°.

Why do the eddies respond differently to north–south shifts of the jet (EOF1) than to strengthening/weakening of the jet (EOF2)? In particular, why does the eddy response to EOF1 have an important component that reinforces EOF1 while the eddy response to EOF2 causes a poleward drift of the wind anomalies? Following previous arguments (e.g., section 6), one would expect a positive feedback for EOF2 also: a stronger temperature gradient in the region of positive wind anomalies implies more wave generation in this region. The propagation of wave activity from this region then reinforces the wind anomalies. The difference between EOF1 and EOF2, however, is that the horizontal shear of EOF2 is coincident with the horizontal shear of the time mean midlatitude jet while for EOF1 it is not. Therefore EOF2

⁴ The factor 1.5 comes from the ratio of the “no feedback” spectrum to the EOF2 spectrum. The factor 2.1 is not the same as the previous 2.1 but is the ratio of total variance of EOF1 to EOF2. Thus, note that 2.1 also equals the ratio of percent variance explained by the EOF’s, i.e., $2.1 = 43\%/21\%$.

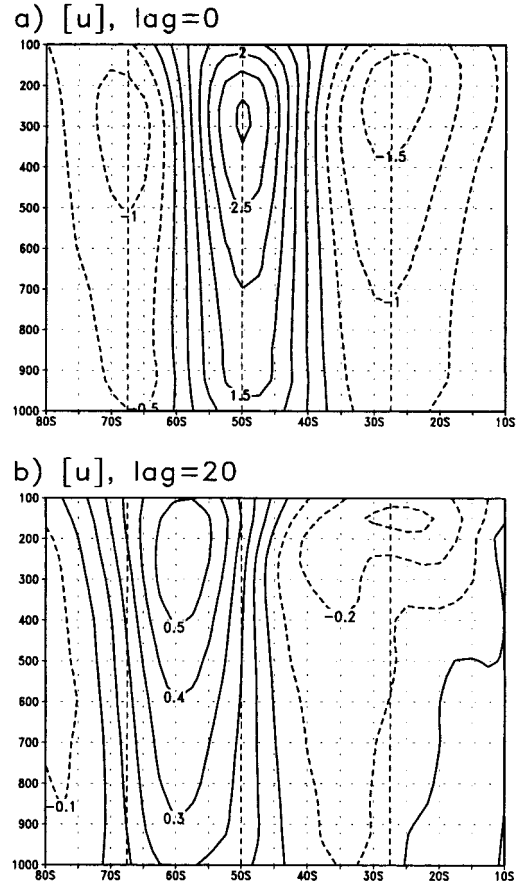


FIG. 15. Anomalous zonal-mean zonal wind regressed on PC2 of $\langle [u] \rangle$: (a) simultaneous and (b) PC2 leads by 20 days; latitudes of the EOF2 wind anomalies are marked by vertical dashed lines.

involves changes in the strength of the barotropic shear on the flanks of the jet. Since increased barotropic shear on the flanks of a baroclinic jet suppresses baroclinic wave growth (see James 1987, section 4), the changes in barotropic shear associated with EOF2 oppose the changes in baroclinicity. Thus the horizontal shear weakens the baroclinic positive feedback and is consistent with the observed result of no positive feedback. For a spherical earth, the above scenario is altered because the effect of anticyclonic (cyclonic) shear reinforces (opposes) the effect of the spherical geometry on the eddies. Thus, on a sphere, the effect of a stronger (weaker) barotropic jet on the fastest growing normal modes is a poleward (equatorward) shift of the eddy fluxes of heat and momentum (see Robinson 1997, end of section 3). The effect of these eddy fluxes on EOF2 is a poleward propagation of the wind anomalies (for both a stronger and a weaker jet). Additional experiments (Robinson 1997) suggest that the key to the poleward shift in the normal mode eddy fluxes is the strengthening of the anticyclonic shear on the equatorward flank of the jet. The asymmetry between the effects of cyclonic and anticyclonic shear on the eddies be-

comes even more pronounced after nonlinearity becomes important (Simmons and Hoskins 1980; Thorncroft et al. 1993; Dong and James 1997; Hartmann and Zuercher 1998; Hartmann 2000).

8. Conclusions

The dominant mode of variability of the zonal-mean zonal wind in the Southern Hemisphere is an equivalent barotropic dipole with opposite anomalies at 40° and 60°S, which represents the north–south displacement of the midlatitude jet. The zonal wind anomalies associated with this mode are driven by eddy momentum flux anomalies. Most of the anomalous eddy forcing is independent of the zonal wind anomalies. However, at low frequencies a significant portion of the eddy forcing is caused by the changes in the zonal-mean wind. These eddy momentum flux anomalies feed back on the zonal wind anomalies and increase the persistence of this leading mode. A simple linear model estimates that this positive feedback is responsible for half of the low-frequency variance of EOF1. Moreover, an analysis of the second EOF, which represents the strengthening/weakening of the jet, suggests that the positive feedback is unique to EOF1 and accounts for the increased persistence of EOF1 compared to EOF2. Also, this positive feedback plays an important role in the selection of the leading mode of midlatitude zonal-mean variability, especially on month-to-month timescales.

The eddy feedback does not project completely on the leading EOF wind anomalies, instead, the feedback consists of two parts: 1) a positive feedback that projects onto EOF1 and 2) a propagating feedback that is in quadrature with EOF1 and implies poleward propagation of the wind anomalies. The magnitude of these two components is roughly the same for EOF1. The positive feedback is unique to EOF1, whereas the propagating feedback is also shared by EOF2.

To help understand the dynamics of the positive feedback, the eddy components of the zonal and meridional wind were divided into high- and low-frequency parts. The high-frequency eddies, which are typically associated with synoptic-scale baroclinic waves, are responsible for the positive feedback on the zonal index. The mechanism of the feedback is as follows. The source of baroclinic wave activity follows the north–south movement of the midlatitude baroclinic jet. The propagation of wave activity away from the jet gives momentum fluxes into the jet. Furthermore, the bias toward equatorward wave propagation contributes to the poleward drift of the wind anomalies and the remote effect of the zonal index in subtropics.

The authors plan to extend the analysis of this paper to the Northern Hemisphere where both stationary and transient eddies play an important role in the momentum budget. In addition, further work is necessary to understand the dynamics involved in the selection of the dominant mode of variability. In particular, why

do the eddies feed back on wind anomalies associated with north–south displacements of the midlatitude jet and not on the strengthening/weakening of the midlatitude jet?

Further insight into the nature of the zonal index may be gained by considering a two layer quasigeostrophic (QG) model on a β plane (perhaps the simplest model that contains the essential dynamics of the midlatitudes). The modeling study of Panetta (1993) demonstrates that quasigeostrophic flow in the presence of a background potential vorticity (PV) gradient organizes itself into zonal jets and storm tracks in the absence of boundaries or inhomogeneities in the forcing. Within a certain parameter range, the flow is characterized by the concentration of the meridional gradients of temperature and upper-level PV into strong eastward jets (much like the midlatitude troposphere) separated by regions of weaker westward flow. (Note that the strong thermal gradient across the jet is not a reflection of the external forcing but of the concentrating effect of the eddies on a broad baroclinic region.) The prominent form of low-frequency variability in these simulations is the meridional wandering of the zonal-mean jets and their associated storm tracks on very long timescales, much like the observed zonal index. In fact, a QG β -plane model with a wide unstable region (but not wide enough for multiple jets) was the focus of the zonal index study of Lee and Feldstein (1996). They found that the “zonal index” was the dominant EOF of the zonal-mean wind for all but the narrowest baroclinically unstable region. Thus, the dominance of the zonal index depends on the existence of a relatively uniform external diabatic forcing. With uniform forcing, the zonal jet and the accompanying synoptic eddies that maintain the jet can persist for long time periods away from the mean latitude. It is this unusual persistence that increases the low-frequency variance of the zonal index and thus plays an important role in the selection of the leading mode. The freedom of zonal jets to move in latitude may be important in climate change (e.g., Thompson et al. 2000; Hartmann et al. 2000). Moreover, the uniformity of external forcing may explain the greater prominence of the zonal index in mechanistic models with a simple relaxation to a smooth temperature profile compared to the atmosphere with its less uniform SST gradients and, in the Northern Hemisphere, with its strong land–sea contrasts.

Acknowledgments. We would like to thank Steven Feldstein, J. M. Wallace, and an anonymous reviewer for their helpful comments and suggestions on the manuscript. Thanks also to the Climate Diagnostics Center for making the NCEP reanalysis data freely available over the World Wide Web. This research was funded by the Climate Dynamics Program of the National Science Foundation under Grant Number ATM-9873691.

APPENDIX A

Estimation of τ

Let Z and M be the Fourier transform of z and m , respectively. If (2) holds, then the ratio of the cross spectrum to the z power spectrum, the transfer function from Z to M , is given by

$$\frac{ZM^*}{ZZ^*} = \frac{1}{\tau} + i\omega, \tag{A1}$$

where $*$ denotes the complex conjugate. The observed real and imaginary part of the transfer function is plotted in Fig. 3a. Like (A1) the imaginary part is linear in frequency and the real part is nearly constant for very low frequencies (at higher frequencies the imaginary part dominates so that the noise in the real part at higher frequencies is not important). We fit the observed transfer function to

$$\frac{ZM^*}{ZZ^*} = \alpha + i\beta\omega. \tag{A2}$$

Since the modeled feedback is proportional to z , the changes in Z and M caused by the feedback are significant at very low frequencies only. Therefore, in order to best estimate the change due to the feedback, we fit the transfer function to $\alpha + i\beta\omega$ for low frequencies ($<0.025 \text{ day}^{-1}$) and not the entire frequency domain. The results are $\alpha = 0.106$ and $\beta = 0.940$. Since we are only interested in the changes in Z and M relative to observed, we can divide (A2) by β and absorb the factor β into M . Thus the value for τ is $\beta/\alpha = 8.9$ days.

APPENDIX B

Statistical Significance of Cross Correlation

To assess the statistical significance in Fig. 5, we perform a Monte Carlo simulation to test following null hypothesis: the cross correlation is zero for large positive lags. To perform this test, we generate a random m dataset using a moving average model (see von Storch and Zwiers 1999). The generated dataset has the same autocorrelation as the real m up to lag 6 and then is exactly zero afterward (this is the same point where the real m autocorrelation appears to be negligible). Thus the generated m has no long-term memory, which is equivalent to the absence of feedback. We then generate a very large dataset using (2) to find the corresponding z . Next, we calculate 1000 independent cross correlations using chunks of z and m that are 20 years long (same as observed data record) and find the standard deviation of the sample cross correlations at large positive lags. This gives a 95% significance level of 0.029 so that the observed cross correlation is significantly different from zero for lags 6–13.

APPENDIX C

Feedback Calculations

To estimate the strength of the feedback, we must find the cross-covariance between \tilde{z} and \tilde{m} from the cross-covariance between z and m using (2), (3), and (4). First we take the Fourier transform of (2), (3), and (4) and rearrange to get

$$M = (\tau^{-1} + i\omega)Z, \tag{C1}$$

$$M = \tilde{M} + bZ, \tag{C2}$$

$$\tilde{M} = (\tau^{-1} + i\omega)\tilde{Z}, \tag{C3}$$

where a capital letter denotes the Fourier transform of the corresponding lowercase variable. Dividing (C1) by (C3) gives

$$\frac{M}{\tilde{M}} = \frac{Z}{\tilde{Z}}. \tag{C4}$$

Substituting (C2) into (C1) and rearranging implies $\tilde{M} = (\tau^{-1} - b + i\omega)Z \equiv (\sigma^{-1} + i\omega)Z$, where σ^{-1} is defined to be $\tau^{-1} - b(1/\tau > b > 0)$. Dividing this result by (C3) and rearranging gives

$$\tilde{Z} = \frac{\sigma^{-1} + i\omega}{\tau^{-1} + i\omega}Z. \tag{C5}$$

The same relation holds between \tilde{M} and M because of (C4):

$$\tilde{M} = \frac{\sigma^{-1} + i\omega}{\tau^{-1} + i\omega}M. \tag{C6}$$

The cross-covariance between \tilde{z} and \tilde{m} [$=c_{\tilde{z}\tilde{m}}(t)$] is the inverse Fourier transform of the cross-spectrum:

$$\begin{aligned} c_{\tilde{z}\tilde{m}}(t) &= \int_{-\infty}^{\infty} \tilde{z}(s)\tilde{m}(s+t) ds \\ &= \frac{1}{2\pi} \int_{-\infty}^{\infty} \tilde{Z}^*(\omega)\tilde{M}(\omega)e^{i\omega t} d\omega. \end{aligned} \tag{C7}$$

Substituting (C5) and (C6) into (C7) implies

$$c_{\tilde{z}\tilde{m}}(t) = \frac{1}{2\pi} \int_{-\infty}^{\infty} \frac{\sigma^{-2} + \omega^2}{\tau^{-2} + \omega^2} Z^* M e^{i\omega t} d\omega. \tag{C8}$$

Using the relationship $1/2\pi \int_{-\infty}^{\infty} F^*(\omega)G(\omega)e^{i\omega t} d\omega = \int_{-\infty}^{\infty} f(s)g(s+t) ds$ from Fourier theory [this is the same as (C7) for general functions f and g] with $F^*(\omega) = (\sigma^{-2} + \omega^2)/(\tau^{-2} + \omega^2)$ and $G(\omega) = Z^*M$ gives

$$\begin{aligned} c_{\tilde{z}\tilde{m}}(t) &= \int_{-\infty}^{\infty} \left[\delta(s) - \frac{\tau}{2}(\tau^{-2} - \sigma^{-2}) \exp\left(\frac{-|s|}{\tau}\right) \right] \\ &\quad \times c_{zm}(s+t) ds, \end{aligned} \tag{C9}$$

where $\delta(s)$ is the Dirac delta function, and where we used the fact that $c_{zm}(t)$ is the inverse Fourier transform of Z^*M . Evaluating the first part of (C9) and performing a change of variables on the second gives

$$c_{\bar{z}\bar{m}}(t) = c_{zm}(t) - b(1 - b\tau/2) \times \int_{-\infty}^{\infty} \exp(-|t - s|/\tau) c_{zm}(s) ds, \quad (\text{C10})$$

where we used the fact that $\sigma^{-1} \equiv \tau^{-1} - b$. To relate the cross correlation with and without the feedback, note that $c_{zm}(t) = \{c_{zz}(0)c_{mm}(0)\}^{1/2}\hat{c}_{zm}(t)$, where $\hat{c}_{zm}(t)$ is the cross correlation, $c_{zz}(0)$ is the total variance of z , etc. Thus (C10) becomes

$$\hat{c}_{\bar{z}\bar{m}}(t) = \left\{ \frac{c_{zz}(0)c_{mm}(0)}{c_{\bar{z}\bar{z}}(0)c_{\bar{m}\bar{m}}(0)} \right\}^{1/2} \times \left\{ \hat{c}_{zm}(t) - b \left(1 - \frac{b\tau}{2} \right) \times \int_{-\infty}^{\infty} \exp\left(-\frac{|t - s|}{\tau}\right) \hat{c}_{zm}(s) ds \right\}. \quad (\text{C11})$$

The relationship between the variance of \bar{z} and z and between the variance of \bar{m} and m is easy to find from the above results because (C5) and (C6) are the same form. Thus (C10) also holds for $c_{\bar{z}\bar{z}}(t)$ and $c_{\bar{m}\bar{m}}(t)$. For zero lag this implies

$$c_{\bar{z}\bar{z}}(0) = c_{zz}(0) - b(1 - b\tau/2) \times \int_{-\infty}^{\infty} \exp(-|s|/\tau) c_{zz}(s) ds, \quad (\text{C12})$$

$$c_{\bar{m}\bar{m}}(0) = c_{mm}(0) - b(1 - b\tau/2) \times \int_{-\infty}^{\infty} \exp(-|s|/\tau) c_{mm}(s) ds. \quad (\text{C13})$$

For the results in this paper, (C10) is used to find the value of b that minimizes the mean square covariance at lags greater than 7 days for $c_{\bar{z}\bar{m}}(t)$. Then (C12) and (C13) are used to find the ratio of total variance between the observed and no feedback case. With this information, (C11) can be used to find the cross correlation without the feedback. The integrals are evaluated from -30 to 30 days with daily resolution using Simpson's rule.

The power spectra for \bar{z} and \bar{m} are easily found from the power spectra of z and m using (C5) and (C6):

$$\tilde{Z}\tilde{Z}^* = \frac{\sigma^{-2} + \omega^2}{\tau^{-2} + \omega^2} ZZ^*, \quad (\text{C14})$$

$$\tilde{M}\tilde{M}^* = \frac{\sigma^{-2} + \omega^2}{\tau^{-2} + \omega^2} MM^*. \quad (\text{C15})$$

APPENDIX D

Fraction of Simultaneous Covariance Caused by Zonal Wind Anomalies

The simultaneous covariance between z and m is

$$\int_{-\infty}^{\infty} zm dt = \int_{-\infty}^{\infty} z \left(\frac{dz}{dt} + \frac{z}{\tau} \right) dt = \frac{1}{\tau} \int_{-\infty}^{\infty} z^2 dt, \quad (\text{D1})$$

where we used (2) for step one and we used the fact that z and the z tendency are in quadrature for the second step. According to the parameterization, the simultaneous covariance between z and the part of m caused by z (i.e., $b \cdot z$) is

$$\int_{-\infty}^{\infty} zbz dt = b \int_{-\infty}^{\infty} z^2 dt. \quad (\text{D2})$$

The fraction of simultaneous covariance caused by the changes in the zonal wind is (D2) divided by (D1) or $b\tau$. The same result holds for composites of eddy forcing when z exceeds a certain threshold because the average wind tendency during these periods is zero.

REFERENCES

- Akahori, K., and S. Yoden, 1997: Zonal flow vacillation and bimodality of baroclinic eddy life cycles in a simple global circulation model. *J. Atmos. Sci.*, **54**, 2349–2361.
- Balasubramanian, G., and S. T. Garner, 1997: The role of momentum fluxes in shaping the life cycle of a baroclinic wave. *J. Atmos. Sci.*, **54**, 510–533.
- Dong, B., and I. N. James, 1997: The effect of barotropic shear on baroclinic instability. Part I: Normal mode problem. *Dyn. Atmos. Oceans*, **25**, 143–167.
- Eady, E. T., 1949: Long waves and cyclone waves. *Tellus*, **1**, 35–52.
- Edmon, H. J., B. J. Hoskins, and M. E. McIntyre, 1980: Ellipsoidal–Palm cross sections for the troposphere. *J. Atmos. Sci.*, **37**, 2600–2616; Corrigendum, **38**, 1115.
- Feldstein, S. B., 1998: An observational study of the intraseasonal poleward propagation of zonal mean flow anomalies. *J. Atmos. Sci.*, **55**, 2516–2529.
- , and S. Lee, 1996: Mechanisms of zonal index variability in an aquaplanet GCM. *J. Atmos. Sci.*, **53**, 3541–3555.
- , and —, 1998: Is the atmospheric zonal index driven by an eddy feedback? *J. Atmos. Sci.*, **55**, 3077–3086.
- Gong, D., and S. Wang, 1999: Definition of Antarctic oscillation index. *Geophys. Res. Lett.*, **26**, 459–462.
- Hamming, R. W., 1989: *Digital Filters*. Prentice Hall, 284 pp.
- Hartmann, D. L., 1995: A PV view of zonal flow vacillation. *J. Atmos. Sci.*, **52**, 2561–2576.
- , 2000: The key role of lower-level meridional shear in baroclinic wave life cycles. *J. Atmos. Sci.*, **57**, 389–401.
- , and F. Lo, 1998: Wave-driven zonal flow vacillation in the Southern Hemisphere. *J. Atmos. Sci.*, **55**, 1303–1315.
- , and P. Zuercher, 1998: Response of baroclinic life cycles to barotropic shear. *J. Atmos. Sci.*, **55**, 297–313.
- , J. M. Wallace, V. Limpasuvan, D. W. J. Thompson, and J. R. Holton, 2000: Can ozone depletion and global warming interact to produce rapid climate change? *Proc. Natl. Acad. Sci.*, **97**, 1412–1417.
- Hoskins, B. J., 1983: Theory of transient eddies. *Large-Scale Dynamical Processes in the Atmosphere*, B. J. Hoskins and R. P. Pearce, Eds., Academic Press, 169–199.

- James, I. N., 1987: Suppression of baroclinic instability in horizontally sheared flows. *J. Atmos. Sci.*, **44**, 3710–3720.
- , and P. M. James, 1992: Spatial structure of ultra-low frequency variability of the flow in a simple atmospheric circulation model. *Quart. J. Roy. Meteor. Soc.*, **118**, 1211–1233.
- Kalnay, M. E., and Coauthors, 1996: The NCEP/NCAR 40-Year Reanalysis Project. *Bull. Amer. Meteor. Soc.*, **77**, 437–471.
- Karoly, D. J., 1990: The role of transient eddies in the low-frequency zonal variations in the Southern Hemisphere circulation. *Tellus*, **42A**, 41–50.
- Kidson, J. W., 1988: Indices of the Southern Hemisphere zonal wind. *J. Climate*, **1**, 183–194.
- , and M. R. Sinclair, 1995: The influence of persistent anomalies on Southern Hemisphere storm tracks. *J. Climate*, **8**, 1938–1950.
- Lee, S., and S. B. Feldstein, 1996: Mechanisms of zonal index evolution in a two-layer model. *J. Atmos. Sci.*, **53**, 2232–2246.
- Limpasuvan, V., and D. L. Hartmann, 1999: Eddies and the annular modes of climate variability. *Geophys. Res. Lett.*, **26**, 3133–3136.
- , and —, 2000: Wave-maintained annular modes of climate variability. *J. Climate*, **13**, 4414–4429.
- Namias, J., 1950: The index cycle and its role in the general circulation. *J. Meteor.*, **7**, 130–139.
- Nigam, S., 1990: On the structure of variability of the observed tropospheric and stratospheric zonal-mean wind. *J. Atmos. Sci.*, **47**, 1799–1813.
- North, G. R., T. L. Bell, R. F. Cahalan, and F. J. Moeng, 1982: Sampling errors in the estimation of empirical orthogonal functions. *Mon. Wea. Rev.*, **110**, 699–706.
- Panetta, R. L., 1993: Zonal jets in wide baroclinically unstable regions: Persistence and scale selection. *J. Atmos. Sci.*, **50**, 2073–2106.
- Robinson, W. A., 1991: The dynamics of the zonal index in a simple model of the atmosphere. *Tellus*, **43A**, 295–305.
- , 1994: Eddy feedbacks on the zonal index and eddy–zonal flow interactions induced by zonal flow transience. *J. Atmos. Sci.*, **51**, 2553–2562.
- , 1996: Does eddy feedback sustain variability in the zonal index? *J. Atmos. Sci.*, **53**, 3556–3569.
- , 1997: Dissipation dependence of the jet latitude. *J. Climate*, **10**, 176–182.
- , 2000: A baroclinic mechanism for the eddy feedback on the zonal index. *J. Atmos. Sci.*, **57**, 415–422.
- Rossby, C.-G., 1939: Relation between variations in the intensity of the zonal circulation of the atmosphere and the displacements of the semi-permanent centers of action. *J. Mar. Res.*, **2**, 38–55.
- Simmons, A. J., and B. J. Hoskins, 1980: Barotropic influences on the growth and decay of nonlinear baroclinic waves. *J. Atmos. Sci.*, **37**, 1679–1684.
- Sinclair, M. R., J. A. Renwick, and J. W. Kidson, 1997: Low-frequency variability of Southern Hemisphere sea level pressure and weather system activity. *Mon. Wea. Rev.*, **125**, 2531–2543.
- Thompson, D. W. J., and J. M. Wallace, 2000: Annular modes in the extratropical circulation. Part I: Month-to-month variability. *J. Climate*, **13**, 1000–1016.
- , —, and G. C. Hergerl, 2000: Annular modes in the extratropical circulation. Part II: Trends. *J. Climate*, **13**, 1018–1036.
- Thorncroft, C. D., B. J. Hoskins, and M. E. McIntyre, 1993: Two paradigms of baroclinic-wave life-cycle behaviour. *Quart. J. Roy. Meteor. Soc.*, **119**, 17–55.
- Trenberth, K. E., 1979: Interannual variability of 500 mb zonal mean flow in the Southern Hemisphere. *Mon. Wea. Rev.*, **107**, 1515–1524.
- von Storch, H., and F. W. Zwiers, 1999: *Statistical Analysis in Climate Research*. Cambridge University Press, 494 pp.
- Whitaker, J. S., and C. Snyder, 1993: The effects of spherical geometry on the evolution of baroclinic waves. *J. Atmos. Sci.*, **50**, 597–612.
- Willett, H. C., 1948: Patterns of world weather changes. *Trans. Amer. Geophys. Union*, **29**, 803–809.
- Yu, J.-Y., and D. L. Hartmann, 1993: Zonal flow vacillation and eddy forcing in a simple GCM of the atmosphere. *J. Atmos. Sci.*, **50**, 3244–3259.